Propagation-invariant wave fields with finite energy

Rafael Piestun

E. L. Ginzton Laboratory, Stanford University, Stanford, California 94305-4085

Yoav Y. Schechner and Joseph Shamir

Department of Electrical Engineering, Technion–Israel Institute of Technology, Haifa 32000, Israel

Received May 6, 1999; revised manuscript received October 5, 1999; accepted October 8, 1999

Propagation invariance is extended in the paraxial regime, leading to a generalized self-imaging effect. These wave fields are characterized by a finite number of transverse self-images that appear, in general, at different orientations and scales. They possess finite energy and thus can be accurately generated. Necessary and sufficient conditions are derived, and they are appropriately represented in the Gauss–Laguerre modal plane. Relations with the following phenomena are investigated: classical self-imaging, rotating beams, eigen-Fourier functions, and the recently introduced generalized propagation-invariant wave fields. In the paraxial regime they are all included within the generalized self-imaging effect that is presented. In this context we show an important relation between paraxial Bessel beams and Gauss–Laguerre beams. © 2000 Optical Society of America [S0740-3232(00)00502-0]

OCIS codes: 030.4070, 050.1960, 110.6760, 140.3300, 350.5030, 350.5500, 350.7420.

1. INTRODUCTION

The understanding and control of waves in free-space propagation is important for many practical situations related, for example, to delivery of information, beam shaping, resonators, or interferometry. Recent research has uncovered new invariance properties of scalar and vector waves that open new possibilities in applications related to this field.[1–18]

A notable manifestation of propagation invariance is the self imaging effect, which is characterized by a repetition of the transverse intensity distribution of the wave along the direction of propagation. General conditions for self-imaging, valid for coherent wave fields (WF's) that satisfy the Helmholtz equation, have been presented in Ref. 19. The corresponding waves present a longitudinally periodic complex amplitude, have infinite transverse extension, and carry infinite energy.[20] Approximate finite aperture implementations of quasi-periodic objects have been widely studied.[2,21–24] The concept of self-imaging was extended recently to include polychromatic light,[4] partial coherence,[7] vector fields,[13] finite-energy waves,[14] and rotated self-images.[16]

In this paper we present paraxial waves that exhibit a generalized self-imaging (GSI), in which the repeated images may be scaled or rotated relative to one another.[1] These waves possess finite energy and thus are an extension of those presented in Ref. 14. In addition, they generalize, within the paraxial regime, the concept of rotated self-imaging presented in Ref. 16.

2. STATEMENT OF THE PROBLEM

Let us consider a monochromatic scalar WF in free space:

$$\mathcal{U}(\mathbf{r}, t) = U(\mathbf{r})\exp(-i\omega t), \tag{1}$$

where $\mathbf{r} \equiv (\rho, \phi, z)$ are the cylindrical coordinates of a point in space, t denotes the time, and ω is the angular temporal frequency. $\mathcal{U}(\rho, \phi, z, t)$ satisfies the appropriate homogeneous wave equation. The GSI problem that we consider is defined as follows: Determine the field in the plane $z = z_1$, $f(\rho, \phi) = U(\rho, \phi, z_1)$, such that at a different location $z = z_2$ the field intensity distribution is reproduced except for possible scaling and rotation transformations.

Apparently, the problem could be formulated as the search for solutions of an eigenfunction equation of the form

$$\mathcal{O}f = \mu f, \tag{2}$$

where the complex number μ is the eigenvalue and the operator $\mathcal{O}$ is defined according to the specific physical approximations. It is composed of a diffraction propagator multiplied by rotation, scaling, and phase operators:

$$\mathcal{O} = \mathcal{P}\mathcal{S}[s]\mathcal{R}[\gamma]\mathcal{D}[\Delta z], \tag{3}$$

where $\mathcal{D}$ is the appropriate diffraction operator, $\Delta z \equiv z_2 - z_1$, $\mathcal{P}$ is a phase operator $\mathcal{P} = \exp[i\Phi(\rho, \phi)]$, $\mathcal{S}$ is a scaling operator $\mathcal{S}[s]g(\rho, \phi) = g(s\rho, \phi)$, and $\mathcal{R}$ is a rotation operator $\mathcal{R}[\gamma]g(\rho, \phi) = g(\rho, \phi + \gamma)$. To gain more generality, we do not constrain *a priori* the phase function $\mathcal{P}$, since only the intensity is of concern here. Therefore we introduce the following nonlinear equation:

$$|\mathcal{O}f|^2 = |\mu f|^2. \tag{4}$$

This is no longer a linear eigenfunction equation. In the following sections we solve it by using expansions of the field complex amplitude in the modes of propagation.

In the context of this paper we deal with paraxial waves, i.e., with spatial frequencies (ξ) vanishing for ξ

0740-3232/2000/020294-10$15.00

$> \xi_0$, where $\xi_0 \ll 1/\lambda$ and λ is the wavelength. Therefore the operator $\mathcal{D}[\Delta z]$ can be expressed as follows:

$$\mathcal{D}[\Delta z] = \mathcal{F}^{-1} \exp\left\{ ik\left[1 - \frac{(\lambda\xi)^2}{2}\right]\Delta z\right\}\mathcal{F}, \tag{5}$$

where $\mathcal{F}$ is the Fourier transform (FT) operator, ξ is the polar spatial frequency, and $k = 2\pi/\lambda$ is the wave number. This operator is equivalent to the Fresnel diffraction operator.[25,26] The wave functions whose intensity distribution is conserved (up to scaling) upon propagation $\mathcal{D}$ are the modal solutions of the paraxial wave equation, e.g., the Gauss–Hermite (GH) and Gauss–Laguerre (GL) modes.[26,27]

3. GAUSS–LAGUERRE MODES

Let us now consider propagating scalar waves represented by the function

$$\mathcal{U}(\mathbf{r}, t) = u(\mathbf{r})\exp[i(kz - \omega t)]. \tag{6}$$

In the paraxial regime the reduced wave field, $u(\mathbf{r})$, can be expanded in terms of GL modes. We represent the GL modes as follows[12,28]:

$$u_{nm}(\mathbf{r}) = G(\hat{\rho}, \hat{z})R_{nm}(\hat{\rho})\Phi_m(\phi)Z_n(\hat{z}), \tag{7}$$

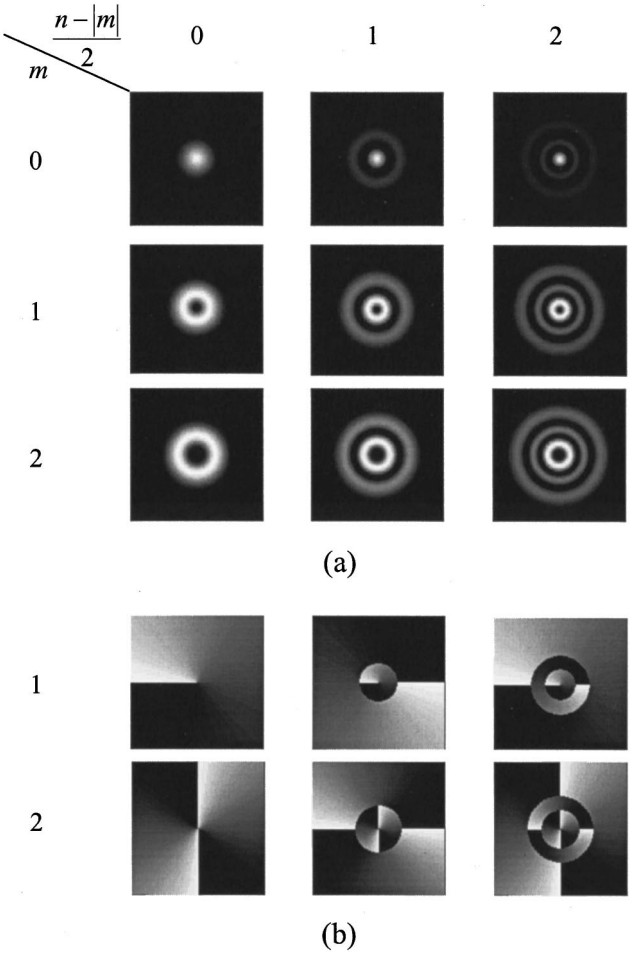

Fig. 1. Examples of GL modes: (a) intensity, (b) phase.

where $\hat{\rho} = \rho/w(\hat{z})$ is the radial coordinate scaled by the Gaussian spot size, given by $w(\hat{z}) = w_0[1 + \hat{z}^2]^{1/2}$. $\hat{z} \equiv z/z_0$ is the longitudinal coordinate scaled by the Rayleigh length, $z_0 = \pi w_0^2/\lambda$. The functions that compose $u_{nm}(\mathbf{r})$ are

$$G(\hat{\rho}, \hat{z}) = \frac{w_0}{w(\hat{z})}\exp(-\hat{\rho}^2)\exp(i\hat{\rho}^2\hat{z})\exp[-i\psi(\hat{z})], \tag{8}$$

$$R_{nm}(\hat{\rho}) = (\sqrt{2}\hat{\rho})^{|m|}L^{|m|}_{(n-|m|)/2}(2\hat{\rho}^2), \tag{9}$$

$$\Phi_m(\phi) = \exp(im\phi), \tag{10}$$

$$Z_n(\hat{z}) = \exp[-in\psi(\hat{z})], \tag{11}$$

where $\psi(\hat{z}) = \arctan(\hat{z})$ is the Gouy phase. The function $G(\hat{\rho}, \hat{z})$ is common to all modes and includes the radial Gaussian envelope of the beam, a quadratic phase, and the Gouy phase. $L^{|m|}_{(n-|m|)/2}$ are the generalized Laguerre polynomials, where the integers n, m satisfy

$$n = |m|, \quad |m| + 2, \quad |m| + 4, \quad |m| + 6, \ldots . \tag{12}$$

These modes form an orthogonal basis. Figure 1 shows the intensities and phase profiles of various GL modes. As n grows, the effective width of the beams grows. m determines the order of the phase singularity at the center of the beam,[29,30] i.e., the number of 2π phase jumps about the central point on a transverse plane. The number of radial zeros is fixed by the number of zeros of the Laguerre polynomial $(n-|m|)/2$ in addition to the central vortex that appears when $m \neq 0$. Hence the total number of bright lobes (including the central one, if applicable) is $1 + (n-|m|)/2$.

We define the effective width of a GL beam as the standard deviation of the intensity distribution[28]:

$$\langle(\Delta x)^2\rangle = \frac{\int\int_{-\infty}^{\infty} x^2 u u^* \mathrm{d}x\mathrm{d}y}{\int\int_{-\infty}^{\infty} u u^* \mathrm{d}x\mathrm{d}y}. \tag{13}$$

The effective half-angular beam spread for a GL beam (θ_{beam}) can be calculated from this definition, leading to

$$\tan(\theta_{\mathrm{beam}}) = \sqrt{n + 1}(\lambda/\pi w_0). \tag{14}$$

Note that the angular spread increases monotonically with n and thus the accuracy of the paraxial approximation becomes poorer as n grows.

4. GAUSS–LAGUERRE MODAL PLANE

Every paraxial WF can be expressed as a weighted combination of the GL basis functions, in a way similar to the decomposition of a function into harmonics. In optics it is useful to decompose a wave front in the spectrum of plane waves that is basically a Fourier transformation of its complex amplitude. The spectrum of plane waves is used to perform calculations of the propagated wave front or to analyze its properties, as in the case of the classical self-imaging effect.

When performing a modal decomposition of the wave front, we propose to present the information in a *modal plane* or *modal domain*. The result is a discrete number of coefficients associated with a discrete set of points in

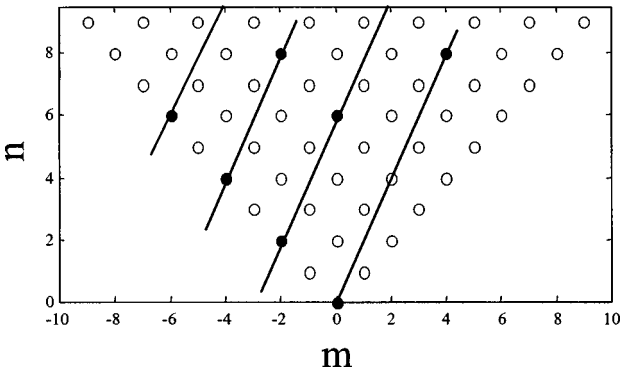

Fig. 2. GL modal domain and generalized self-imaging: Each mode that composes the wave is represented by a point within a grid. The support of generalized self-imaging waves lies upon uniformly spaced parallel lines (see text).

this modal plane (Fig. 2). This information is useful for performing wave-front propagation calculations by simply superposing the propagated GL modes [according to Eq. (7)]. In addition, we shall see below that this representation is also useful in visualizing important properties of the WF. Therefore the GL representation is a natural and convenient representation of wave fronts that possess finite effective width. In such a representation, however, the beam waist and its location are parameters that must be optimized for an efficient expansion with a small number of nonzero coefficients. Although some studies have been performed, the optimization of this process remains an unsolved problem.[26]

5. CONDITION FOR GENERALIZED SELF-IMAGING

In this section we investigate superpositions of GL modes that present a GSI effect, i.e., WF's that are solutions of an equation of the type of Eq. (4). We obtain powerful necessary and sufficient conditions that are useful for the analysis and synthesis of WF's and show that interesting phenomena can be predicted.

Let us consider a superposition of GL modes:

$$u(\mathbf{r}) = \sum_{j=1}^{Q} A_j u_{n_j,m_j}(\mathbf{r}), \tag{15}$$

where A_j is the complex amplitude of mode j. Without loss of generality we can assume that $n_j \leqslant n_{j+1}$. Thus the intensity distribution is given by

$$I(\mathbf{r}) = |G(\hat{\rho})|^2 \Bigg\{ \sum_{j=1}^{Q} |A_j|^2 R^2_{n_j,\,m_j}(\hat{\rho}) + \sum_{j=1}^{Q} \sum_{p=j+1}^{Q} 2|A_j||A_p| R_{n_j,m_j}(\hat{\rho}) R_{n_p,m_p}(\hat{\rho}) \times \cos[\Delta m_{jp}\phi - \Delta n_{jp}\psi(\hat{z}) - \theta_{jp}] \Bigg\}, \tag{16}$$

where $\Delta m_{jp} \equiv m_j - m_p$, $\Delta n_{jp} \equiv n_j - n_p$, and $\theta_{jp} \equiv [\arg(A_j) - \arg(A_p)]$.

We consider a GSI scaled as the elementary Gaussian spot size; i.e., the magnification between self-images is

$$s = \frac{w(\hat{z}_2)}{w(\hat{z}_1)} = \left(\frac{1 + \hat{z}_2^2}{1 + \hat{z}_1^2} \right)^{1/2}. \tag{17}$$

Condition (4) is thus

$$|u(\rho,\, \phi,\, z_1)|^2 = \left| \mathcal{S}\left[\frac{w(\hat{z}_2)}{w(\hat{z}_1)} \right] \mathcal{R}[\gamma] \mathcal{D}[\Delta z] u(\rho,\, \phi,\, z_1) \right|^2, \tag{18}$$

leading to

$$I(\hat{\rho},\, \phi,\, z_1) = I(\hat{\rho},\, \phi + \gamma,\, z_2) \tag{19}$$

for all $\hat{\rho}$, ϕ.

The first sum on the right-hand side of Eq. (16) is self-imaged (except for scale) because it does not depend on $\hat{z}$. The second sum is composed of terms that represent waves rotating linearly with $\psi(\hat{z})$.[12] Therefore Eq. (19) will be fulfilled if each of the corresponding terms is equal at z_1 and z_2:

$$\cos[\Delta m_{jp}\phi - \Delta n_{jp}\psi(\hat{z}_1) - \theta_{jp}] = \cos[\Delta m_{jp}(\phi + \gamma + 2\pi N) - \Delta n_{jp}\psi(\hat{z}_2) - \theta_{jp}]. \tag{20}$$

The functions that multiply the cosine functions depend on $\hat{\rho}$ through $R_{n_j,m_j}(\hat{\rho})$ and $R_{n_p,m_p}(\hat{\rho})$. Consequently, the equality of each term is a necessary condition to satisfy Eq. (19). Thus Eq. (20) is also a necessary as well as a sufficient condition for Eq. (19) to be satisfied.

Equation (20) is satisfied for all ϕ if and only if

$$\Delta m_{jp}\phi - \Delta n_{jp}\psi(\hat{z}_1) - \theta_{jp} = \Delta m_{jp}(\phi + \gamma + 2\pi N) - \Delta n_{jp}\psi(\hat{z}_2) - \theta_{jp} + 2\pi N' \tag{21}$$

for all ϕ, j, p, leading to

$$\Delta n_{jp}\Delta\psi = \Delta m_{jp}\gamma + 2\pi N_{jp} \tag{22}$$

for all j, p, where N_{jp} is any integer and

$$\Delta\psi = \psi(\hat{z}_2) - \psi(\hat{z}_1). \tag{23}$$

Equation (22) is satisfied if and only if the indices n_j, m_j of each mode j that compose the wave satisfy

$$n_j = n_1 + \frac{\gamma(m_j - m_1) + 2\pi N_j}{\Delta\psi} \tag{24}$$

for all j, where n_1, m_1, and N_j are integers. n_1, m_1 are arbitrary as long as they satisfy Eq. (12).

It is easy to show that, when $N_j \neq 0$ for some j, $\Delta\psi/(2\pi)$ must be a rational number. However, this is not a significant limitation, as we show in Section 7. In addition, in these cases the fraction of a complete rotation $(\gamma/2\pi)$ is also a rational number.

Although we required GSI only between two planes, Eq. (20) shows that the scaled rotated transverse intensity distribution is periodic in $\psi(\hat{z})$ along the propagation axis. In addition, since $\psi(\hat{z})$ is bounded, the number of periods is finite. Moreover, in some cases there might not even be a complete period. This is a remarkable extension of the classical self-imaging effect, for which the WF's are periodic along the propagation direction *(z)*.

Condition (24) can be better understood when viewed in the modal GL plane (see Fig. 2). It states that in an ap-

propriate GL basis, GSI WF's present modes that lie on a set of parallel lines at ordinate distances $2\pi/\Delta\psi$ and are inclined at an angle $\arctan(\gamma/\Delta\psi)$ with respect to the m axis. Note that there is a reciprocal relation between the ordinate distance between the lines in the GL plane [Eq. (22)] and the distance between the self-images in the axial direction. Note also that the angle of rotation is proportional to the slope of the lines.

6. PHASE RELATION BETWEEN SELF-IMAGES

We have shown the existence of waves that present the same transverse intensity distribution (with different scales and orientations) at various locations along the propagation. In the following we investigate the phase relation between these intensity self-images. The amplitude of the wave given in Eq. (15) at $(\hat{\rho}, \phi, z_1)$ is

$$u(\hat{\rho}, \phi, \hat{z}_1) = \frac{w_0}{w(\hat{z}_1)} \exp(-\hat{\rho}^2)\exp[-i(1 + n_1)\psi(\hat{z}_1)] \times \exp(i\hat{\rho}^2\hat{z}_1)\exp(i m_1\phi)\sum_{j=1}^{Q} A_j R_j(\hat{\rho}) \times \exp\{i[(m_j - m_1)\phi - (n_j - n_1)\psi(\hat{z}_1)]\}, \tag{25}$$

and at $(\hat{\rho}, \phi + \gamma, z_2)$ it is

$$u(\hat{\rho}, \phi + \gamma, z_2) = \frac{w_0}{w(\hat{z}_2)} \exp(-\hat{\rho}^2) \times \exp[-i(1 + n_1)\psi(\hat{z}_2)] \times \exp(i\hat{\rho}^2\hat{z}_2)\exp[i m_1(\phi + \gamma)] \times \sum_{j=1}^{Q} A_j R_j(\hat{\rho})\exp\{i[(m_j - m_1) \times (\phi + \gamma) - (n_j - n_1)\psi(\hat{z}_2)]\}. \tag{26}$$

Because of the orthogonality of the modes, the sums that appear in Eqs. (25) and (26) are equal if and only if each of the corresponding terms is equal in the planes at $\hat{z}_1$ and $\hat{z}_2$. This leads directly to condition (24). Alternatively, we can substitute Eq. (24) and get an identity between the sums that appear in Eqs. (25) and (26).

Therefore the two-dimensional scaled phase distributions are related by

$$\arg[u(\hat{\rho}, \phi + \gamma, \hat{z}_2)] = \arg[u(\hat{\rho}, \phi, \hat{z}_1)] + m_1\gamma - (1 + n_1)\Delta\psi + (\hat{z}_2 - \hat{z}_1)\hat{\rho}^2. \tag{27}$$

Thus the phase map of the wave (scaled and rotated) is self-reproduced with the intensity distribution, except for the quadratic-radial term $(\hat{z}_2 - \hat{z}_1)\hat{\rho}^2$ and a constant $[m_1\gamma - (1 + n_1)\Delta\psi]$.

7. GENERAL CHARACTER OF THE GENERALIZED SELF-IMAGING CONDITION

The condition of Eq. (24) is general in the sense that it applies to every paraxial wave that exhibits GSI with any magnification and between any two planes. To prove this, we must find at least one suitable GL basis in which these conditions can be applied, i.e., a location for the fundamental Gaussian beam waist and its width. Let us assume that the distance between the planes is $\Delta z \equiv z_2 - z_1$ and that the magnification is s.

If $s = 1$, then, from Eq. (17), $z_1 = -\Delta z/2$, and z_0 can be arbitrarily chosen. Otherwise, if $s \neq 1$, from Eq. (17) we obtain

$$z_0^2 + z_1^2 - \frac{2\Delta z}{s^2 - 1}z_1 - \frac{\Delta z^2}{s^2 - 1} = 0, \tag{28}$$

that is, the equation of a circle in the (z_1, z_0) plane. The condition $z_0 \geqslant 0$ leaves a circular arc as the solution to this equation. This is the domain of $\Delta\psi$, which is a function of (z_0, z_1). The next step is to prove that there is at least one pair (z_0, z_1) that leads $\Delta\psi/(2\pi)$ to assume a rational number, a necessary condition that should be satisfied according to Eq. (24). This is possible, in fact, since $\Delta\psi = \Delta\psi(z_0, z_1)$ is continuous and nonconstant in this domain. Thus it is always possible to choose a pair (z_0, z_1) to make $\Delta\psi/(2\pi)$ a rational number, i.e., to satisfy Eq. (24) and at the same time satisfy Eq. (17). It should be noted, however, that there is still a great deal of freedom in analyzing and synthesizing the self-imaging objects. That is, once Δz and s are given, there is an infinite number of legitimate values of z_0 and z_1 for which condition (24) is satisfied.

We define an appropriate basis as one that provides the required magnification between the two planes under consideration. Note that condition (24) can be applied only after an appropriate basis is set, because $\Delta\psi$ depends on the choice of z_0 and z_1; this may be interpreted as a weakness of this formulation.

8. RELATED PHENOMENA OF PROPAGATION INVARIANCE

Various wave phenomena related to the GSI presented here have been reported.[2,3,11,12,14,16] Since some of these WF's are solutions of the full Helmholtz equation, they can lead to either paraxial or nonparaxial waves. We show below that, in the former case, the GSI waves include all the other phenomena as particular cases. Some of these phenomena are included as limiting cases for which the energy of the paraxial GSI waves tend to infinity. In what follows, we characterize all these phenomena and their interrelations, but first we need to prove an important relation between paraxial Bessel modes and GL beams.

A. Relation between Gauss–Laguerre and Paraxial Bessel Beams

We show here that under given conditions a GL mode tends to a paraxial Bessel mode. We choose a limit at which the effective width and the number of lobes of the GL mode tend to infinity while still being within the

paraxial regime. An important by-product of this limiting process is that it shows us the way to approximate a superposition of (infinite energy) Bessel beams by a superposition of beams with finite energy; i.e., each Bessel beam is approximated, within an arbitrary large central region, by a corresponding GL beam with large enough effective width.

We perform the limiting process by taking (see Appendix A for further explanation)

$$z/z_0 \to 0, \qquad \rho/w_0 \to 0, \qquad n \to \infty,$$
$$n - |m| \approx n, \qquad \lambda\sqrt{n}/w_0 \leqslant C^2 = \text{const.}, \tag{29}$$

and then a GL mode u_{nm} [Eq. (7)] is transformed as follows (see Appendix A):

$$u_{nm}^{\text{limit}}(\mathbf{r}) = c(m) J_{|m|}\left(\frac{2\sqrt{n}\rho}{w_0}\right)\exp(im\phi)\exp\left(-i\frac{z}{z_0}n\right), \tag{30}$$

where $c(m)$ is constant for a given mode and J_m denotes a Bessel function of order m. Defining $\alpha \equiv 2\sqrt{n}/w_0$, we obtain

$$u_{nm}^{\text{limit}}(\mathbf{r})\exp[i(kz - \omega t)] = c(m) J_{|m|}(\alpha\rho)\exp(im\phi) \times \exp\left[i\left(k - \frac{\alpha^2}{2k}\right)z\right] \times \exp(-i\omega t), \tag{31}$$

which is a general Bessel beam[3,5] in the paraxial approximation, i.e., with

$$\beta \equiv \sqrt{k^2 - \alpha^2} \approx k\left(1 - \frac{\alpha^2}{2k^2}\right). \tag{32}$$

B. Generalized Propagation-Invariant Wave Fields

The GPI fields presented in Ref. 16 satisfy a general concept of propagation invariance in the sense that self-images may present azimuthal changes. Although those GPI fields are similar to the GSI waves introduced here, they differ in various ways: (1) They are solutions of the full Helmholtz equation, and thus they apply to both paraxial and nonparaxial cases; (2) they do not present scale changes; (3) self-images repeat indefinitely along the propagation direction; and (4) they carry infinite energy. The last two properties stem from the fact that GPI WF's possess an infinite effective width.

It is then interesting to see when the GSI waves and the GPI WF's are equivalent. Obviously, this happens when the GSI waves possess infinite effective width and the GPI waves satisfy the paraxial condition. In other words, infinite effective width GSI WF's are paraxial GPI WF's and vice versa. In what follows, we show that indeed this is the case.

First we recall that the GPI WF's are composed of a superposition of Bessel modes with propagation constants β that satisfy the relation[16]

$$\beta = \beta_{m,N} = \beta_0 - \frac{m\gamma + 2\pi N}{\Delta z}, \qquad 0 \leqslant \beta \leqslant k, \tag{33}$$

where N and m are integers restricted by the above bounds on β. β_0 is real, γ is the rotation between self-images, and Δz is the axial distance.[31] Note that Eq. (33) is a necessary and sufficient condition.

We now consider a superposition of GL modes that satisfy the conditions of Eq. (29) in addition to the condition for GSI [Eq. (24)]. From relations (31) and (32) we obtain $\beta = k - n/z_0$. Note also that under the limiting conditions of relation (29), $\Delta\psi \approx \Delta z/z_0$. Then, by substituting n according to Eq. (24), we get[32]

$$\beta = \left(k - \frac{n_1}{z_0} + \frac{\gamma m_1}{\Delta z}\right) - \frac{m\gamma + 2\pi N}{\Delta z}. \tag{34}$$

This is equivalent to Eq. (33) with $\beta_0 = k - (n_1/z_0) + (\gamma m_1/\Delta z)$.

Note that β_0 satisfies the condition $0 \leqslant \beta_0 < k$, while the value $\beta_0 = k$ corresponds to a plane wave for which the limit in Eq. (31) does not apply. Nevertheless, it is clear that the fundamental Gaussian beam satisfies

$$u_{00} \xrightarrow{\rho/w_0 \to 0} 1, \tag{35}$$

leading to a plane wave.

In summary, we have shown limiting conditions that led from condition (24) to the solutions of Eq. (33). Therefore Eq. (24) contains the solutions of the GPI WF's in the paraxial case. Note that the nonparaxial GPI WF's are not included in condition (24), and the finite effective width (and energy) GSI waves are not included in condition (33).

C. Scaled Self-Imaging

In Ref. 14 we presented necessary and sufficient conditions for self-imaging waves of finite energy. It is apparent that from Eq. (24), with γ=0, we get the same condition for scaled self-imaging:

$$n_j = n_1 + \frac{2\pi N_j}{\Delta\psi} \qquad \text{for all } j, \tag{36}$$

where n_1 and N_j are integers. In this case the condition depends only on the parameter n of the modes, i.e., on the factor of the Gouy phase. In the modal plane, scaled self-imaging waves are represented as a set of lines parallel to the m axis, separated by distances $2\pi N_j/\Delta\psi$ [Fig. 3(a)]. With the additional condition of Eq. (36), $m_j = m_1$ for all j, we obtain the class of scaled self-imaging waves with rotational symmetry of the intensity distribution.

In the interesting special case when $z_1 = -z_2$ there is self-imaging between planes located symmetrically on both sides of the basic Gaussian beam waist. Then $s = 1$, and there is no scaling. In addition, based on the properties of the GL modes, it is easy to show that

$$u(\rho, \phi, z_1) = u(\rho, \phi, z_2)^*, \tag{37}$$

i.e., the self-imaged amplitudes are complex conjugates of each other. Therefore we shall call this effect phase-conjugate self-imaging.

The particular case $n_j = n_1$ for all j (that is, $\Delta n_{jp} = 0$ for all j, p) is also interesting since it leads to the complete class of eigenmodes for which the intensity distribution is preserved independently of z, as can be deduced from Eq.

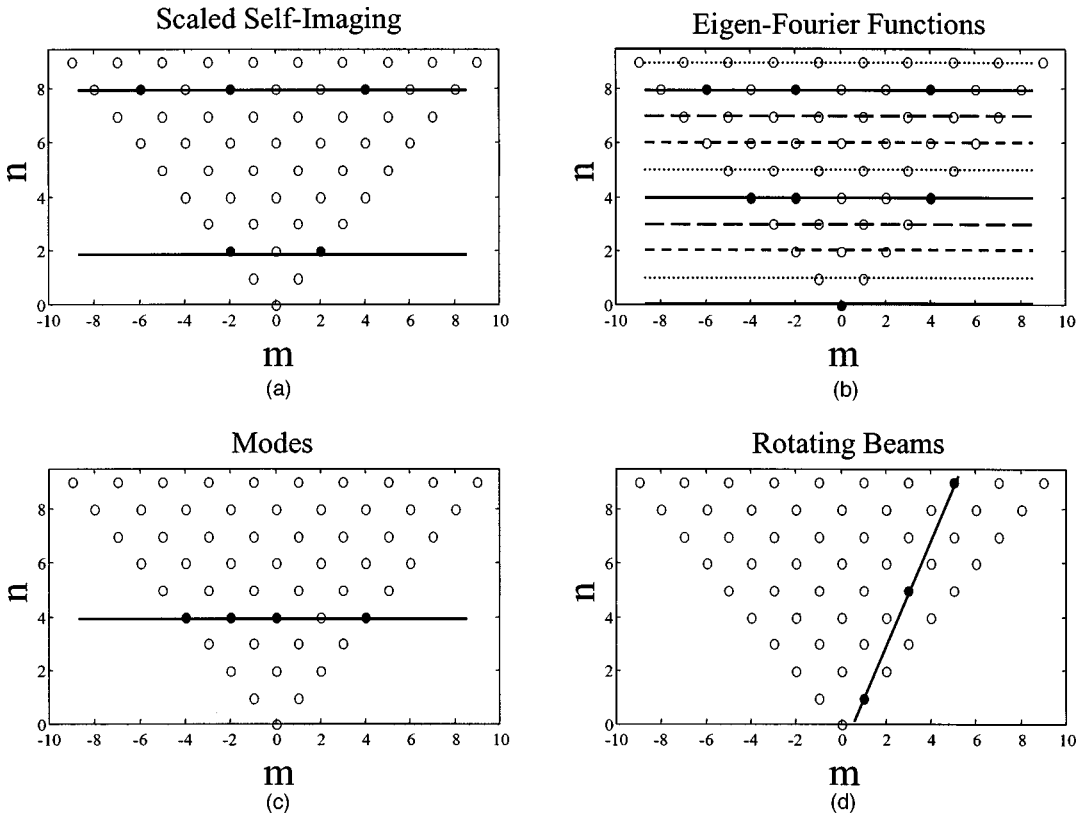

Fig. 3. Particular cases of the GSI waves: (a) Scaled self-imaging waves have GL modes lying on horizontal parallel lines. (b) Eigen-Fourier functions generate waves that are self-reproduced in the far field, with GL modes lying on parallel lines at a distance 4, leading to four possible families depicted by different dashed lines. (c) A mode possesses an invariant transverse intensity distribution during propagation; all the constituent GL modes have the same n number. (d) Rotating beams are composed of GL modes lying on a single line.

(16) [Fig. 3(c)]. Note that these modes can be quite different from the GL or GH basis functions.

A similar approach may be used to obtain a self-imaging condition for expansions in GH modes. It is worth noting also that GL modes can be expressed as superpositions of GH modes with $n_x + n_y = n$,[33] and therefore condition (36) can be directly applied to GH modes.

D. Eigen-Fourier Functions

Consider a set of functions that can be defined as eigen-Fourier functions that satisfy the relation

$$\mathcal{F}f = \mu f. \tag{38}$$

The FT relations require that

$$\mu^4 = 1 \Rightarrow \mu = \exp(iL\pi/2), \quad L = 0, 1, 2, \ldots, \tag{39}$$

which leads to four eigenvalues. Consequently there are four independent sets of eigenfunctions (one for each eigenvalue). The complete set of eigen-Fourier functions is defined by the following generating formula:

$$f(\mathbf{x}) = \exp(ia)g(\mathbf{x}) + G(\mathbf{x}) + \exp(i3a)g(-\mathbf{x}) + \exp(i2a)G(-\mathbf{x}), \tag{40}$$

where $a = L\pi/2$ and $G = \mathcal{F}g$, with g an arbitrary two-dimensional complex function. This condition is necessary and sufficient for $f(\mathbf{x})$ to be an eigen-Fourier function. Note that, given f, the decomposition of Eq. (40) is not unique. A subset of these solutions contains the self-FT functions[34–38] with eigenvalue $\mu = 1$.

To include the eigen-Fourier functions as a special case of GSI we consider WF's with the intensity distribution self-reproduced in the far field, while the phase map differs only in a quadratic phase, as explained in Section 6. If the self-imaging occurs between the beam waist of the fundamental GL mode and the far field, the solutions of eigenfunction Eq. (2) are, except for phase and scale changes, the eigen-Fourier functions. From Eq. (27), with $\Delta\psi = \pi/2$ and $\gamma = 0$, we see that the eigenvalues are

$$u = \exp[i(1 + n_1)\pi/2] = i^{(1+n_1)}, \tag{41}$$

with n_1 an integer. In particular, the self-Fourier functions are obtained for $n_1 = 3 + 4L$, $L = 0, 1, 2, \ldots$. Equation (36) with $\Delta\psi = \pi/2$ dictates that

$$n_j = n_1 + 4N_j \qquad \text{for all } j. \tag{42}$$

We see that indeed there are four independent sets of solutions, each with a corresponding different n_1 and consequently a different eigenvalue. The eigenvalues are consistent with those derived mathematically for eigen-Fourier functions in relation (39). This is also seen in the modal plane, where there are four possible sets of horizontal lines [Fig. 3(b)].

We can also define the eigenrotated FT functions by the relation

$$\mathcal{R}[\gamma]\mathcal{F}f = \mu f; \tag{43}$$

then the modal condition of Eq. (24) leads to

$$n_j = n_1 + \frac{2\gamma}{\pi}(m_j - m_1) + 4N_j \qquad \text{for all } j. \tag{44}$$

E. Rotating Beams

Another notable manifestation of the GSI effect occurs when the transverse intensity distribution is invariant upon propagation, except for a possible continuous rotation about the axis. In Ref. 12 we presented the complete class of paraxial coherent rotating beams by showing necessary and sufficient conditions and an experimental demonstration. Related investigations appeared in Refs. 1, 11, and 15–18. Additional properties of rotating beams can be derived in the present framework by solving the operator equation

$$|u(\rho, \phi, z_1)|^2 = \left|\mathcal{S}\left[\frac{w(z)}{w(z_1)}\right]\mathcal{R}[\gamma(z)]\mathcal{D}[z - z_1]u(\rho, \phi, z_1)\right|^2 \tag{45}$$

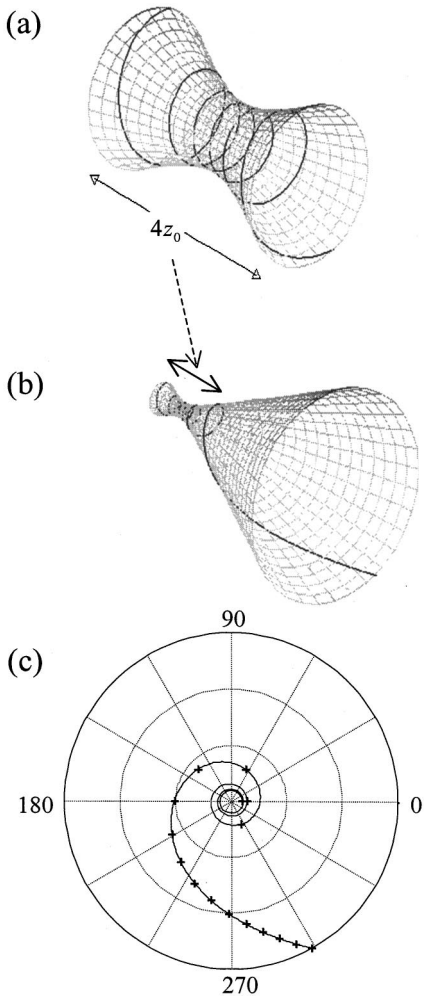

Fig. 4. Spiral trajectory of a point in the transverse intensity distributions of a rotating beam. (a) Detail of the waist, showing maximal rotation rate. (b) Coarser view of the spiral, showing that the rotation rate tends to zero toward the far field. (c) Projection of the spiral onto a transverse plane. The axial distance between consecutive marks (+) is z_0.

for every z and with $\gamma(z)$ denoting a continuous function of z.

Let us examine a superposition of modes as in Eq. (16). Each term in the second sum represents a wave rotating linearly with $\psi(\hat{z})$ at the spatial rotation rate

$$\left(\frac{d\phi}{d\hat{z}}\right)_{jp} = \frac{\Delta n_{jp}}{\Delta m_{jp}}\frac{d\psi(\hat{z})}{d\hat{z}}. \tag{46}$$

Terms that have $m_j = m_p$ are isotropic, so they will not be considered further. If all of these waves rotate at the same rate, rotation of the scaled transverse intensity distribution will be observed. Mathematically this means that $(d\phi/dz)_{jp}$ is independent of j, p. This is the case when $\Delta n_{jp}/\Delta m_{jp}$ = constant for all j, p, leading to

$$n_j = V_1 m_j + V_2, \qquad j = 1, 2, \ldots, \tag{47}$$

where V_1 and V_2 are constants. If Eq. (47) is not fulfilled, additional harmonics will appear in the rotation. Hence this is a necessary and sufficient condition for rotation of the scaled transverse intensity distribution. The rotation rate can be derived from this condition as

$$\frac{d\gamma}{d\hat{z}} = \frac{d\phi(\hat{z})}{d\hat{z}} = \frac{\Delta n}{\Delta m}\frac{d\psi(\hat{z})}{d\hat{z}} = \frac{V_1}{1 + \hat{z}^2}. \tag{48}$$

Note that the rotation rate is maximal at the waist and is reduced asymptotically to zero in the far field. Each point in the transverse image describes a spiral trajectory (see Fig. 4) given by

$$\begin{aligned} \rho &= \rho_0\sqrt{1 + \hat{z}^2}, \\ \phi &= \phi_0 + V_1\psi(\hat{z}), \end{aligned} \tag{49}$$

where (ρ_0, ϕ_0) are the coordinates of the point at $z = 0$. The total rotation from the waist ($z = 0$) to the far field ($z = \infty$) is then

$$\Delta\phi_{\text{total}} = V_1(\pi/2), \tag{50}$$

as it is from $z = -\infty$ to the waist. Half of $\Delta\phi_{\text{total}}$ is obtained at the Rayleigh distance.

The rotating beams are a particular case of the WF's defined by condition (24). For $N_j = 0$ we directly obtain condition (47), with $V_1 = \gamma/\Delta\psi$ and $V_2 = n_1 - \gamma m_1/\Delta\psi$, where $\Delta\psi$ and γ are calculated for any two transverse planes. Rotating beams satisfy the GSI criterion between any two specific transverse planes, since taking $\gamma = V_1\Delta\psi$ makes condition (24) valid for any $\Delta\psi$.

Waves with rotating intensity distributions present a GL modal representation confined to a single line [Fig. 3(d)]. The modal plane representation provides an easy way to test the following properties:

- In general, an arbitrary combination of rotating beams is not a rotating beam, since all the modes should lie on the same line to produce a rotating beam.
- Any paraxial WF can be decomposed into a superposition of rotating beams. This decomposition is, in general, not unique.

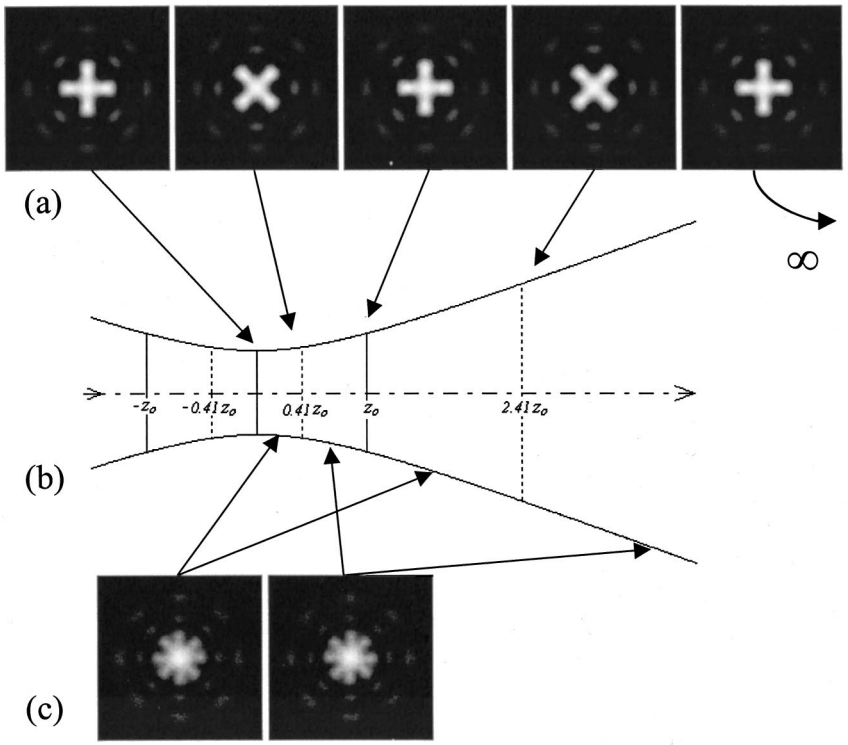

Fig. 5. Example of scale-rotated self-imaging. (a) The transverse intensity distribution is self-reproduced at different positions with different orientations and scales (see text). (b) Representation of the changes of scale along the propagation. (c) The intermediate cross sections are different but are also self-reproduced with scaling and rotation.

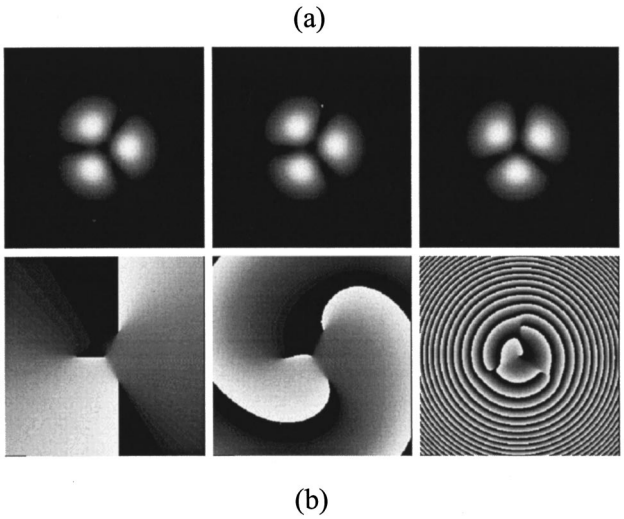

Fig. 6. Example of a rotating beam with an odd azimuthal symmetry. (a) The scaled transverse intensity distribution is invariant on propagation, except for a change in orientation. Note the slow rotation rate that leads to a total rotation of 30° from waist to far field. (b) The phase is invariant on propagation, except for a change in orientation and scale and the addition of a quadratic phase term. Note the rotating (first-order) phase dislocations. From left to right in (a) and (b), $\hat{z} \approx 0$, 0.25, 5.04.

9. EXAMPLES

In this section we present two examples that illustrate the GSI effect. First, we consider a wave composed of a superposition of the following modes: $u_{0,0}$, $u_{8,-4}$, and $u_{8,4}$. At the waist ($z = 0$) the intensity distribution resembles a cross, as shown in Fig. 5. From the GL representation it is easy to observe that the self-images are obtained at $\hat{z} \approx 0.41$, 1, 2.41, ∞ (far field) with successive relative rotations of $\pi/4$ rad. At intermediate planes the intensity distribution is different, as shown in Fig. 5(c). However, these intermediate images are also self-reproduced with relative azimuthal changes of $\pi/4$ rad. For example, at $\hat{z} \approx 0.20$ and 0.67 we observe the images shown in Fig. 5(c), which appear once again on propagation to the far field. In all cases the scale changes obey Eq. (17). In this simple example we observe rotated self-imaging of an eigen-Fourier function.

In the second example, we present a rotating beam. The composing modes are $u_{1,-1}$ and $u_{2,2}$; thus the total rotation from waist to the far field is 30°. Figure 6 shows the scaled intensities and phase distributions at different locations. Note that the scaled phase map is invariant, except for the addition of a quadratic phase and the rotation. Observe the existence of four phase singularities, which ease the perception of the rotation. An interesting property of this beam is that the number of azimuthal lobes is odd, a property that is impossible to achieve with nonrotating modes.

10. DISCUSSION AND CONCLUSIONS

The current approach deals with waves that are exact solutions to the paraxial wave equation. There is no need for further approximations, as in the case of classical self-imaging waves implemented with finite apertures. The solutions composed of superpositions of GL modes fall off rapidly away from the propagation axis and thus limit the

support of the object to an effective finite aperture. Truncation effects can be arbitrarily reduced, producing negligible aberrations on the results.

Typically, the intensity distribution at a certain plane will be imaged at other locations, with different scales and rotation angles. This phenomenon can exist between any two planes, with any magnification, and with any rotation of a rational fraction of 2π. These waves possess finite energy and thus are physically realizable. Equation (24) gives a necessary and sufficient condition for this GSI. The scaled phase map is also replicated, with the exception of a quadratic phase. Usually there is a finite number of self-images spaced nonuniformly along the propagation direction, in contrast to the uniform periodic structure of the classical self-imaging. The intermediate intensity distributions (called Fresnel images in the literature on classical self-imaging) are also self-reproduced. Especially interesting cases include the rotating beams, the eigen-Fourier functions, and the phase conjugate self-imaging. In general, the characteristics of the WF's can be deduced from a graphic representation on the GL plane. Therefore this is an effective and elegant way to represent paraxial waves and their characteristics. Note that the GPI WF's in the paraxial regime are also contained as a limiting case of the present framework.

The physical basis for the rotated self-imaging is explained by the existence of two types of phase: the Gouy phase and the wave-front phase dislocations. The different properties of the GSI waves depend on the existence of phase dislocations (m numbers) and on the envelope of the beam that hosts them and that determines the order of the Gouy phase (n numbers). The ultimate behavior of the beam on propagation is determined by the interrelation among the Gouy and dislocation phases of the composing GL modes (see also Refs. 12 and 16). This interrelation is analytically described by Eq. (24).

The paradigm and approach presented here can be extended to other wave phenomena. Effects similar to those described here for free-space propagation of paraxial waves can be predicted and observed in other circumstances, leading to various possible generalizations. For example, it is well known that any first-order optical system can be described by an integral operator analogous to the Fresnel operator.[26,39] Thus it is possible to extend all the effects described here to the propagation of beams through first-order optical systems. This includes the fractional Fourier transform and the fields that are invariants of this transformation.

Another extension is in the time domain. In this case it is possible to obtain a GSI in time at fixed locations. For this purpose it is necessary to have superpositions of GL modes with different optical frequencies. This can be achieved, for example, with multimode lasers[40] or with a single-mode laser and an acousto-optic modulator.

In addition, GSI effects can also be predicted for guided waves, including gradient-index media. Finally, it is important to note that similar effects may also appear in partially coherent beams,[7,18] and thus it is worth following the research in this direction.

In conclusion, the results presented in this paper provide a framework for understanding, analyzing, and synthesizing propagation-invariant waves.

APPENDIX A

Let us explain the origin of the conditions presented in expression (29):

A. To make the GL modes resemble (infinite) plane waves and Bessel modes, we can reduce the quadratic-radial phase by requiring that $\hat{z} \ll 1$, e.g., with $z_0/\lambda \rightarrow \infty$ and z bounded. Thus we impose $z/z_0 \rightarrow 0$. In order to have an infinite number of lobes, we impose $n \rightarrow \infty$.

B. The effective half-angular beam spread of a GL mode obeys[30]

$$(\pi/\lambda)\tan(\theta_{\text{beam}}) = \frac{\sqrt{n+1}}{w_0} \overset{n\to\infty}{\rightarrow} \frac{\sqrt{n}}{w_0}. \tag{A1}$$

The angular beam spread must be kept small to satisfy the paraxial approximation, in spite of $n \rightarrow \infty$. Therefore

$$\lambda\sqrt{n}/w_0 \leqslant C^2 = \text{const.} \tag{A2}$$

C. To make the GL modes resemble infinite effective width waves, we require ρ to be much smaller than the basic Gaussian beam spot size, w_0: $\hat{\rho} \rightarrow 0$. Note that then $\exp(-\rho^2/w_0^2) \rightarrow 1$.

D. The smaller the difference $n - |m|$, the lower the energy concentrated about the axis (where condition C is valid). Thus, to maintain a significant amount of energy in the axial region, we require that $n \gg |m|$ and thus that $n - |m| \approx n$.

Derivation of Eq. (30): We apply these conditions to Eq. (7) in the following relation[41]:

$$\eta^{-b} L_{\eta}^{b}(\chi/\eta) \overset{\eta\to\infty}{\rightarrow} \chi^{-b/2} J_b(2\sqrt{\chi}), \tag{A3}$$

where J_b denotes a Bessel function of order b and we substitute $\eta = (n - |m|)/2$, $\chi = n\hat{\rho}^2$, and $b = |m|$.

ACKNOWLEDGMENTS

This research was partially supported by the Israeli Ministry of Science and by The Fund for the Promotion of Research at the Technion–Israel Institute of Technology (IIT). Part of this research was performed while R. Piestun was at the Technion–IIT.

REFERENCES AND NOTES

1. Part of this study appeared in R. Piestun, Y. Y. Schechner, and J. Shamir, "Generalized self-imaging in free space," presented at the DO'97, EOS Topical Meeting on Diffractive Optics, Savonlinna, Finland, July 7–9, 1997.
2. K. Patorski, "Self-imaging phenomenon and its applications," in *Progress in Optics*, E. Wolf, ed. (Pergamon, Oxford, UK, 1989), Vol. XXVII, pp. 3–108.
3. J. Durnin, "Exact solutions for nondiffracting beams. I. The scalar theory," J. Opt. Soc. Am. A **4**, 651–654 (1987).
4. G. Indebetouw, "Polychromatic self-imaging," J. Mod. Opt. **35**, 243–252 (1988).
5. G. Indebetouw, "Nondiffracting optical fields: some remarks on their analysis and synthesis," J. Opt. Soc. Am. A **6**, 150–152 (1989).
6. P. Szwaykowski and J. Ojeda-Castaneda, "Nondiffracting beams and the self-imaging phenomenon," Opt. Commun. **83**, 1–4 (1991).

7. J. Turunen, A. Vasara, and A. T. Friberg, "Propagation invariance and self-imaging in variable-coherence optics," J. Opt. Soc. Am. A **8**, 282–289 (1991).
8. G. Indebetouw, "Quasi-self-imaging using aperiodic sequences," J. Opt. Soc. Am. A **9**, 549–558 (1992).
9. V. Yu. Bazhenov, M. S. Soskin, and M. V. Vasnetsov, "Screw dislocations in light wavefronts," J. Mod. Opt. **39**, 985–990 (1992).
10. G. Indebetouw, "Optical vortices and their propagation," J. Mod. Opt. **40**, 73–87 (1993).
11. E. Abramochkin and V. Volostnikov, "Spiral-type beams," Opt. Commun. **102**, 336–350 (1993).
12. Y. Y. Schechner, R. Piestun, and J. Shamir, "Wave propagation with rotating intensity distributions," Phys. Rev. E **54**, R50–R53 (1996).
13. Z. Bouchal, R. Horak, and J. Wagner, "Propagation-invariant electromagnetic fields: theory and experiment," J. Mod. Opt. **43**, 1905–1920 (1996).
14. R. Piestun, Y. Y. Schechner, and J. Shamir, "Self-imaging with finite energy," Opt. Lett. **22**, 200–202 (1997).
15. V. V. Kotlyar, V. A. Soifer, and S. N. Khonina, "An algorithm for the generation of laser beams with longitudinal periodicity: rotating images," J. Mod. Opt. **44**, 1409–1416 (1997).
16. R. Piestun and J. Shamir, "Generalized propagation-invariant wave fields," J. Opt. Soc. Am. A **15**, 3039–3044 (1998).
17. S. N. Khonina, V. V. Kotlyar, V. A. Soifer, M. Honkanen, J. Lautanen, and J. Turunen, "Generation of rotating Gauss–Laguerre modes with binary-phase diffractive optics," J. Mod. Opt. **46**, 227–238 (1999).
18. R. Simon and N. Mukunda, "Iwasawa decomposition in first-order optics: universal treatment of shape-invariant propagation for coherent and partially coherent beams," J. Opt. Soc. Am. A **15**, 2146–2155 (1998).
19. W. D. Montgomery, "Self-imaging objects of infinite aperture," J. Opt. Soc. Am. **57**, 772–778 (1967).
20. W. D. Montgomery, "Algebraic formulation of diffraction applied to self-imaging," J. Opt. Soc. Am. **58**, 1112–1124 (1968).
21. J. M. Cowley and A. F. Moodie, "Fourier images. III. Finite sources," Proc. Phys. Soc. London Sect. B **70**, 505–513 (1957).
22. A. Kalestynski and B. Smolinska, "Self-restoration of the autoidolon of defective periodic objects," Opt. Acta **25**, 125–134 (1978).
23. A. P. Smirnov, "Fresnel images of periodic transparencies of finite dimensions," Opt. Spectrosc. (USSR) **44**, 208–212 (1978).
24. R. Moignard and J. L. de Bougrenet de laTocnaye, "3D self-imaging condition for finite aperture objects," Opt. Commun. **132**, 41–47 (1996).
25. J. W. Goodman, *Introduction to Fourier Optics* (McGraw-Hill, New York, 1996).
26. A. E. Siegman, *Lasers* (University Science, Mill Valley, Calif., 1986).
27. H. Kogelnik and T. Li, "Laser beams and resonators," Proc. IEEE **54**, 1312–1329 (1966).
28. Y. Y. Schechner, "Rotation phenomena in waves," MSc. Thesis (Technion–Israel Institute of Technology, Haifa, Israel, 1996).
29. J. F. Nye and M. V. Berry, "Dislocations in wave trains," Proc. R. Soc. London, Ser. A **336**, 165–190 (1974).
30. Y. Y. Schechner and J. Shamir, "Parameterization and orbital angular momentum of anisotropic dislocations," J. Opt. Soc. Am. A **13**, 967–973 (1996).
31. Note that there is a change of sign in Eq. (33) compared with that equation in Ref. 16. This is simply due to a different convention for the direction of positive rotations (γ).
32. Note that in this case the condition $n \to \infty$ that appears in expression (29) is redundant, since it is implicit in Eq. (24) together with the rest of the conditions of expression (29). In effect, in the limit $(\Delta z/z_0) \to 0$, we obtain a uniform periodicity in z and, according to Eq. (24), for $\gamma = 0$ we have
$$n_j - n_1 \overset{\hat{z}\to 0}{\approx} 2\pi N_j (z_0/\Delta z) \overset{\hat{z}\to 0}{\to} \infty$$
for all j. Thus $n_j \to \infty$.
33. G. Nienhuis and L. Allen, "Paraxial wave optics and harmonic-oscillators," Phys. Rev. A **48**, 656–665 (1993).
34. A. W. Lohmann and D. Mendlovic, "Self-Fourier objects and other self-transform objects," J. Opt. Soc. Am. A **9**, 2009–2012 (1992).
35. M. J. Caola, "Self-Fourier functions," J. Phys. A **24**, L1143–L1144 (1991).
36. S. G. Lipson, "'Self-Fourier objects and other self-transform objects': comment," J. Opt. Soc. Am. A **10**, 2088–2089 (1993).
37. M. W. Coffey, "Self-reciprocal Fourier functions," J. Opt. Soc. Am. A **9**, 2453–2455 (1994).
38. G. Cincotti, F. Gori, and M. Santarsiero, "Generalized self-Fourier functions," J. Phys. A **25**, L1191–L1194 (1992).
39. M. Nazarathy and J. Shamir, "First-order optics—a canonical operator representation: lossless systems," J. Opt. Soc. Am. **72**, 356–364 (1982).
40. G. Slekys, K. Staliunas, and C. O. Weiss, "Motion of phase singularities in a class-B laser," Opt. Commun. **119**, 433–446 (1995).
41. M. Abramowitz and I. A. Stegun, eds. *Handbook of Mathematical Functions* (Dover, New York, 1965).